IFSCC 2025 full paper (856)

A Dual-Component Complex Mitochondrial Flash Charge Cellular Energy Pack: Fast-Acting and Long-Lasting Skin Problem Solution

Yintao Lin [1], Kangjin Zhang [1], Wenyun Zhang [1], Lu Ren [1], Qinrun Lai [1], Yan Ai [1], Xian Xu [1], Yan Huang [2], Tomoko Oto [3,*], Dongcui Li [1,*]

[1] Research and Development, Hua An Tang Biotech Group Co., Ltd., Guangzhou, China ; [2] Key Laboratory for Analytical Science of Food Safety and Biology, Ministry of Education; College of Biological Science & Engineering, Fuzhou University, Fuzhou, China ; [3] Nihon Inemoto Co., LTD, Tokyo, Japan

---

1. Introduction

Mitochondria are dynamic, double-membraned organelles found in eukaryotic cells. Their primary function is the generation of adenosine triphosphate (ATP) through cellular respiration, serving as the main energy source of cells [1]. In addition to energy production, mitochondria play essential roles in regulating cell viability, proliferation, calcium homeostasis, and programmed cell death [2-3]. In the context of skin, mitochondrial function is vital for maintaining cellular vitality, supporting fibroblast proliferation, collagen synthesis, and overall tissue integrity.

However, both internal and external stressors—such as ultraviolet (UV) radiation, alcohol, cigarette smoke and inflammation—can impair mitochondrial function [4-7]. This dysfunction manifests as decreased ATP production, reduced mitochondrial membrane potential (ΔΨm), diminished mitochondrial density, and lower respiratory capacity, particularly in aging cells [8-9]. Such mitochondrial decline contributes to skin aging and imbalance, often resulting in lipid droplet accumulation in adipocytes [10], impaired collagen synthesis in fibroblasts, and pigmentation abnormalities due to altered melanocyte activity [11]. Therefore, preserving mitochondrial function is critical for maintaining the viability and biosynthetic activity of dermal fibroblasts, which are essential for sustaining tissue architecture and overall skin health [12]. Addressing mitochondrial dysfunction is therefore crucial for restoring skin homeostasis and delaying the visible signs of aging. There is a growing demand for innovative and sustainable cosmetic strategies, particularly those based on plant-derived actives that support mitochondrial health in a natural and effective manner. In this study, we investigate the

efficacy of a novel dual-component active complex designed to restore mitochondrial function and promote skin cell balance. This sustainable formulation comprises two key components: (1) a triple plant-derived mixture aimed at enhancing mitochondrial performance, and (2) an accelerator mixture to further boost efficacy. We evaluated the complex's effects on mitochondrial quantity, ΔΨm, and ATP levels in various skin cell types, including human melanocytes, dermal fibroblasts (HSFs), and SZ95 sebocytes. Furthermore, we assessed its influence on cellular homeostasis and functional activities critical for skin health.

2. Materials and Methods

2.1. Materials

The main materials used in the two sample groups—Triple Plant-Derived Mixture (TPM) and Triple Plant-Derived Mixture with Accelerator Mixture (TPM-EX)—were generously provided and listed in Table 1.

Table 1. Composition of the main ingredients in the two sample groups.

Sample group	Main ingredients
Triple plant-derived mixture (TPM)	Haberlea Rhodopensis leaf extract, Myrothamnus Flabellifolia leaf/stem extract, and Selaginella Pulvinata extract
Triple plant-derived mixture and accelerator mixture (TPM-EX)	Haberlea Rhodopensis leaf extract, Myrothamnus Flabellifolia leaf/stem extract, Selaginella Pulvinata extract, carnosine, niacinamide, and sodium mannose phosphate

2.2. Methods

2.2.1. Mitochondrial Membrane Potential (ΔΨm) Assay

Immortalized human keratinocytes (5×10^4 cells/well) were seeded into 12-well plates and cultured at 37℃ in a humidified atmosphere with 5% CO_2 for 24 hours. After removing the culture medium, the cells were washed with D-Hanks solution. The sample and model control groups were then exposed to UVB irradiation (100 mJ/cm²), while the normal control group remained unexposed. Following irradiation, the blank and model control groups were supplemented with fresh medium, whereas the sample and positive control groups were treated with test compounds or a reference drug. After 24 hours of incubation, the cells were stained with JC-1 dye to assess ΔΨm. Fluorescence images were captured, and the red-to-green fluorescence intensity ratio was quantified using Image J Software. The ΔΨm change efficacy was calculated as follows:

$$\Delta\Psi m \text{ red - green fluorescence intensity ratio} = \frac{S\ (\text{Red fluorescence intensity})}{S\ (\text{Green fluorescence intensity})}$$

$$\text{Effect}\ (\%) = \frac{A\ (\text{Sample group}) - A\ (\text{Model control group})}{A\ (\text{Model control group})} \times 100\%$$

A: Red/green fluorescence intensity ratio indicating changes in ΔΨm

2.2.2. ATP Assay

Immortalized human keratinocytes were seeded into 6-well plates at a density of 6×10^5 cells per well and incubated at 37℃ with 5% CO_2 for 24 hours. After incubation, the culture medium was removed, and the cells were washed 1-2 times with D-Hanks solution. Fresh medium

was added to the blank control group, while the sample groups received fresh medium containing the corresponding concentrations of test samples. All groups were then incubated under the same conditions for an additional 24 hours. Subsequently, ATP levels were measured using a commercially available ATP assay kit, following the manufacturer's instructions. The ATP change efficacy was calculated as follows:

$$\text{Effect (\%)} = \frac{\text{A (Sample group)} - \text{A (Blank control group)}}{\text{A (Blank control group)}} \times 100\%$$

A: ATP levels

2.2.3. Mitochondrial Quantity Assay

Human dermal fibroblasts were seeded into 12-well plates at a density of 5×104 cells per well and incubated at 37℃ with 5% CO_2 for 24 hours. After incubation, the culture medium was removed, and the cells were washed 1-2 times with D-Hanks solution. The model control group was replenished with fresh medium containing H_2O_2, the sample groups received fresh medium containing H_2O_2 and the respective test sample, and the positive control group was treated with fresh medium containing H_2O_2 and a positive control agent. All groups were then incubated under the same conditions (37℃, 5% CO_2) for an additional 1 hour. Following incubation, cells were stained with Mito-Tracker Green, a mitochondrial-specific fluorescent probe, and images were captured using a fluorescence microscope. Fluorescence intensity (S) for each group was analyzed using Image J software, and mitochondrial vitality enhancement was calculated.

$$\text{Effect (\%)} = \frac{\text{A (Sample group)} - \text{A (Model control group)}}{\text{A (Model control group)}} \times 100\%$$

A：Fluorescence intensity

2.2.4. Oil-Controlling Efficacy Assay

Cells were seeded into 12-well plates at a density of 1×10^5 cells per well and incubated at 37℃ with 5% CO_2 for 24 hours. After incubation, the blank control group was replenished with fresh medium, the model control group received medium containing testosterone (TE), and the sample control group was treated with medium containing TE and the corresponding concentrations of the test sample. All groups were further incubated under the same conditions (37℃, 5% CO_2) for an additional 24 hours. Following incubation, the medium was removed, and cells were washed 3 times with pre-cooled D-Hanks solution. Cells were then fixed with 60% isopropanol, washed again with D-Hanks, and stained with Nile Red. Fluorescence images were acquired using a fluorescence microscope, and fluorescence intensity was quantified for each group using Image J software for each group. The oil-control efficacy was calculated as follows:

$$\text{Oil control effect (\%)} = \frac{\text{A (Model control group)} - \text{A (Sample group)}}{\text{A (Model control group)}} \times 100\%$$

A：Fluorescence intensity

2.2.5. Type I Collagen Synthesis Assay

Human skin fibroblasts (HSFs) in the mid-to-late logarithmic growth phase were harvested, digested, counted, and seeded into 24-well plates with sterile glass coverslips. After 24 hours of incubation at 37 °C with 5% CO_2, the culture medium was discarded and replaced with corresponding sample solutions according to the experimental design. Cells were incubated for an additional 24 hours. Following PBS washing, cells were exposed to UVA irradiation,

then treated again with respective samples and incubated for another 48 hours. After treatment, cells were fixed with paraformaldehyde, permeabilized with Triton X-100, and blocked with BSA solution. Type I collagen was stained using Rabbit Anti-Collagen I antibody followed by Alexa Fluor® 488-conjugated Goat Anti-Rabbit IgG H&L. After mounting, fluorescence images were acquired using a fluorescence microscope. Image J software was used to measure fluorescence intensity, and corrected total cellular fluorescence (CTCF) was calculated using the following formula:

$$\text{CTCF} = \text{Density (Cumulative)} - \text{Area (Cell to be measured)} \times \text{Optical Density (Background)}$$

$$\text{Relative fluorescence intensity (\%)} = \text{CTCFe/CTCFb} \times 100\%$$

CTCFe: CTCF of groups S, PC and NC, CTCEb: CTCF of groups BC

2.2.6. Whitening Efficacy

The test samples were prepared in aqueous solution and administered at 3 mL per well, with a blank control group included. All groups were incubated in the dark at 28℃ for 45 hours. Following incubation, ten individuals from each group were randomly selected and imaged under a stereomicroscope. Melanin signal intensity (S) was analyzed using image analysis software. Whitening efficacy was assessed based on the calculated reduction in melanin signal according to a defined formula as follows:

$$\text{Whitening effect (\%)} = \frac{\text{S (Normal control group)} - \text{S (Sample group)}}{\text{S (Normal control group)}} \times 100\%$$

2.2.7. In-vivo clinical test

A preliminary in-house clinical trial was conducted with 10 participants (N = 10). A model cosmetic formulation containing 0.5% of the active complex was topically applied to sleep-deprived individuals to simulate stress-induced skin damage. Short-term recovery was evaluated within one hour post-application, focusing on redness reduction and skin hydration. Long-term benefits—including improvements in skin texture, radiance, and overall skin condition—were assessed over a four-week period.

3. Results

3.1. ΔΨm Assay

Red fluorescence indicates JC-1 aggregates that form with mitochondria under high membrane potential, while green fluorescence represents JC-1 monomers dispersed in the cytosol following mitochondrial membrane depolarization. Thus, ΔΨm serves as a key indicator of mitochondrial functional integrity [13]. As shown in Figure 1, the UVB-treated group exhibited a marked reduction in red fluorescence intensity compared to the blank control (BC), indicating a significant mitochondrial depolarization. In contrast, TPM treatment notably preserved mitochondrial integrity following UVB exposure, as evidenced by increased red fluorescence. Both TPM and TPM-EX groups demonstrated a substantial restoration of ΔΨm, with the latter showing enhanced efficacy, suggesting that the accelerator mixture exerted a synergistic protective effect on mitochondrial function.

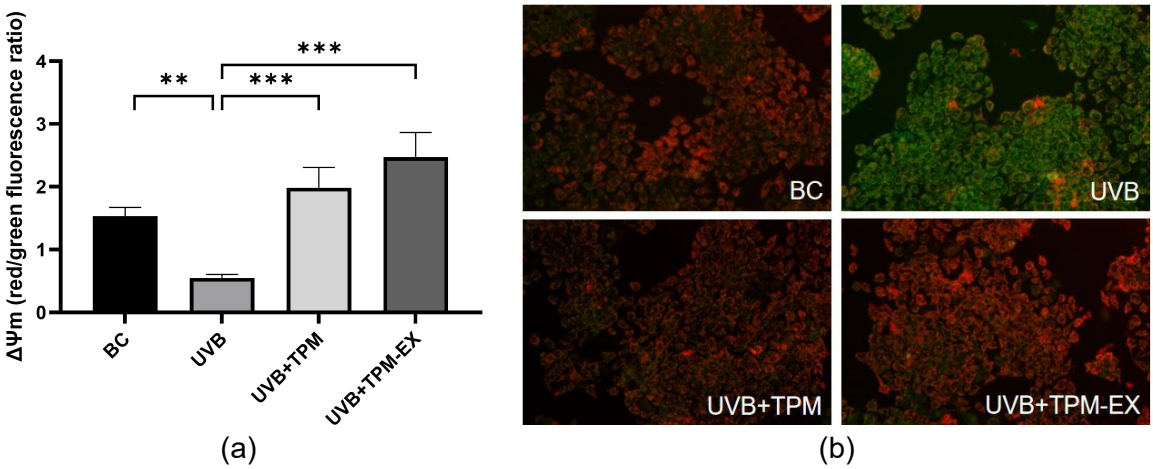

Figure 1. Evaluation of ΔΨm using JC-1 fluorescence. Red fluorescence indicates JC-1 aggregates in polarized mitochondria, while green fluorescence represents JC-1 monomers in depolarized mitochondria. ΔΨm was quantified as the ratio of red to green intensity. (a) Bar graph showing ΔΨm values across different treatment groups. (b) Representative fluorescence images of mitochondria in BC, UVB, UVB+TPM, and UVB+TPM-EX groups. *=p<0.05; **=p<0.01; ***=p<0.001.

3.2. ATP Assay

The accumulation of dysfunctional mitochondria or other damaged organelles can disrupt cellular metabolism and lead to a reduction in ATP production [14]. As illustrated in Figure 2, treatment with both TPM and TPM-EX resulted in a significant increase in mitochondrial ATP levels compared to the control. These findings indicate that the active complex, TPM and TPM-EX, enhances mitochondrial bioenergetic function, thereby supporting the energy demands required for cellular homeostasis and viability. Notably, TPM-EX demonstrated superior efficacy, highlighting the synergistic effect of the accelerator mixture combined with TPM in enhancing mitochondrial function.

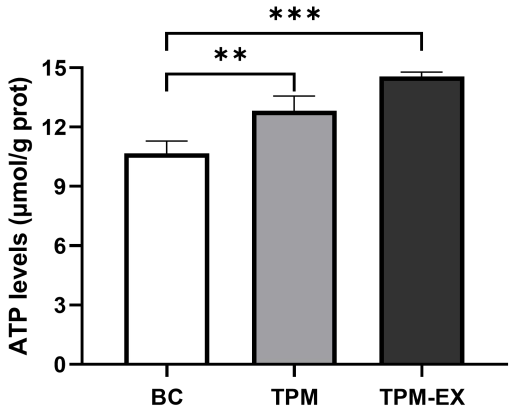

Figure 2. ATP levels in keratinocytes. Keratinocytes cultured under normal conditions served as the blank control (BC). *=p<0.05; **=p<0.01; ***=p<0.001.

3.3. Mitochondrial Quantity Assay

Each cell maintains mitochondrial quantity through a delicate balance between fusion and fission, essential for proper mitochondrial function [15]. The sample treated with H_2O_2 alone exhibited a significant reduction in mitochondrial count compared to the control group. As shown in Figure 3, H_2O_2 disrupts the balance between mitochondrial fusion and fission,

leading to a marked decrease in mitochondrial quantity ($p<0.001$ vs. BC). In contrast, both TPM and TPM-EX treatments resulted in a statistically significant increase in mitochondrial quantity. These treatments effectively restored the balance between mitochondrial fusion and fission, thereby enhancing mitochondrial quantity and function. Notably, TPM-EX demonstrated superior efficacy, further confirming the synergistic effect of the accelerator mixture in enhancing mitochondrial quantity and function.

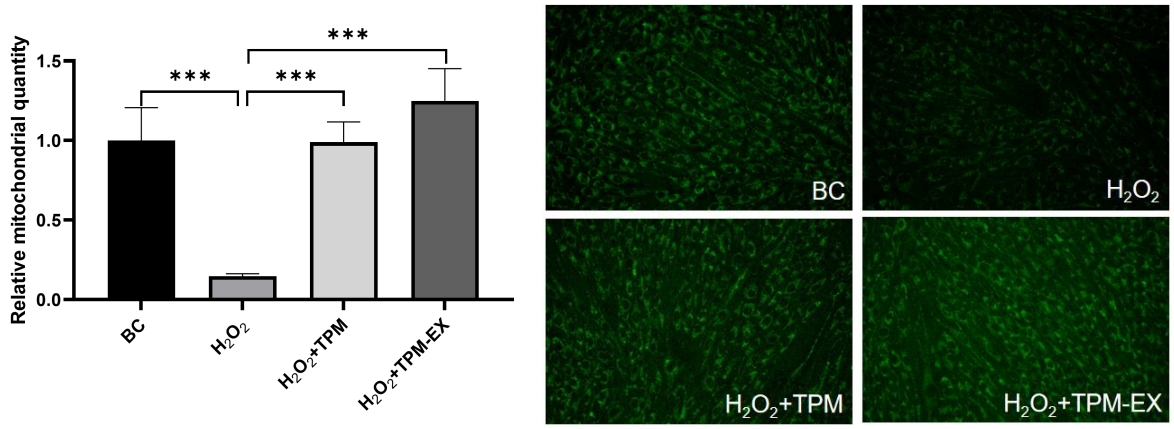

(**a**) (**b**)

Figure 3. Evaluation of mitochondrial quantity by Mito-Tracker Green. Higher green fluorescence intensity indicates greater relative mitochondrial quantity, reflecting increased mitochondrial density within cells. (a) Bar chart comparison of relative mitochondrial quantity in different groups. (b) Fluorescence images of mitochondria in the blank control (BC), H_2O_2, H_2O_2+TPM, and H_2O_2+TPM-EX groups. *=$p<0.05$; **=$p<0.01$; ***=$p<0.001$.

3.4. Oil-controlling efficacy experiment

Testosterone is converted to 5-Dihydrotestosterone (5-DHT), the most potent androgen in target tissues, by 5α-reductase, stimulating sebocytes to increase sebum production [16-17]. As shown in Figure 4, treatment with testosterone (TE) resulted in a significant increase in lipid content within SZ95 sebocytes compared to controls, as indicated by intensified red fluorescence. Both TPM and TPM-EX treatments significantly reduced lipid content compared to the model control group. This reduction was accompanied by a corresponding decrease in red fluorescence intensity, demonstrating the substantial oil-controlling efficacy of the treatments. In vitro mitochondrial assessments combined with theoretical analysis demonstrated that TPM and TPM-EX enhance mitochondrial activity, thereby regulating lipid secretion in SZ95 sebocytes and restoring them to a state of balanced lipid secretion. Notably, TPM-EX exhibited superior efficacy compared to TPM alone, supporting the synergistic role of the accelerator mixture in enhancing lipid regulation.

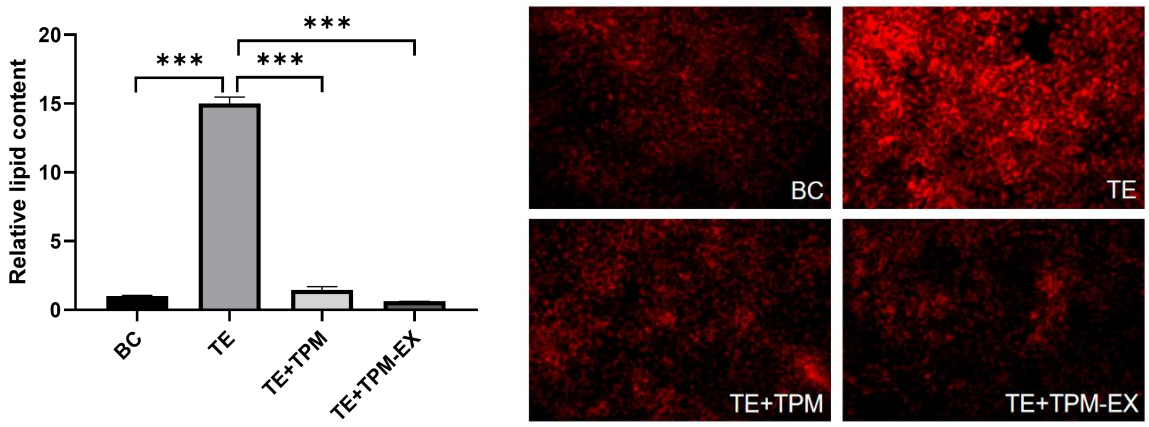

(**a**) (**b**)

Figure 4. Evaluation of lipid content in SZ95 sebocytes using Nile red staining. Reduced red fluorescence intensity indicates lower intracellular lipid accumulation. (a) Bar chart comparing relative lipid content across different groups. (b) Fluorescence images of SZ95 sebocytes from the blank control (BC), TE, TE+TPM, and TE+TPM-EX groups. *=p<0.05; **=p<0.01; ***=p<0.001.

3.5. Type I Collagen Synthesized Assay

Fibroblasts are the principal collagen-producing cells in the dermis and bind to intact collagen fibrils via integrin receptors on their surface [18]. As shown in Figure 5, UVA exposure led to a significant reduction in type I collagen levels compared to the blank control (BC) group, evidenced by diminished green fluorescence. Treatment with TPM and TPM-EX significantly restored collagen levels, indicating potent anti-aging activity. In vitro mitochondrial assessments, together with theoretical analysis, confirmed that both the TPM and TPM-EX enhance mitochondrial function, thereby restoring HSF viability and promoting type I collagen synthesis. Notably, TPM-EX exhibited superior efficacy, supporting the synergistic role of the accelerator in enhancing TPM's biological activity.

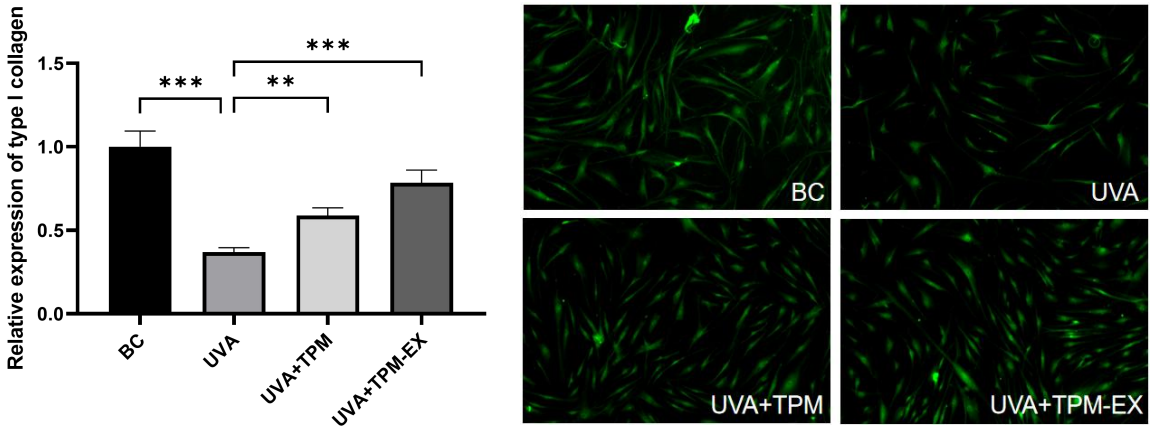

(**a**) (**b**)

Figure 5. Evaluation of type I collagen synthesized by HSFs. (a) Bar chart comparing relative expression of type I collagen across different groups. (b) Fluorescence images of HSFs from the blank control (BC), UVA, UVA+TPM, and UVA+TPM-EX groups. Green fluorescence indicates type I collagen expression levels. *=p<0.05; **=p<0.01; ***=p<0.001.

3.6. Whitening Efficacy

Melanin pigments on the surface enable direct observation of pigmentation dynamics without the need for complicated experimental procedures [19]. As shown in Figure 6, the TPM group exhibited no significant difference in melanin signal intensity compared to the BC group, indicating limited skin-whitening efficacy. In contrast, the TPM-EX group demonstrated a pronounced reduction in melanin signal intensity, not only relative to the BC group but also exceeding the performance of the positive control group. These findings highlight the potent whitening efficacy of the accelerator mixture and underscore its synergistic enhancement of TPM's baseline activity.

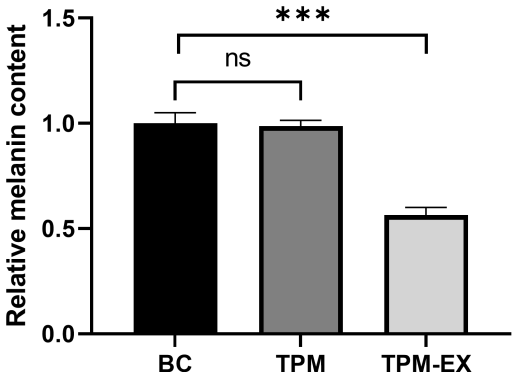

Figure 6. Evaluation of whitening efficacy. Melanin signal intensity was measured to assess pigmentation levels. A lower intensity indicates reduced melanin accumulation and improved whitening. Bar chart comparison of melanin signal intensity in different groups. Normal untreated sample served as the blank control (BC). *=p<0.05; **=p<0.01; ***=p<0.001.

3.7. Clinical trials of TPM and TPM-EX

As shown in Figure 7, one hour after application of cosmetic formulations containing TPM and TPM-EX by sleep-deprived participants (N=10), both skin elasticity and firmness showed notable improvements. TPM-EX demonstrated superior efficacy compared to TPM alone, suggesting a synergistic benefit from the accelerator complex. These results are aligned with the in-vitro results. Furthermore, long-term monitoring over four weeks revealed significant enhancement in multiple skin parameters across all participants, indicating sustained improvement in overall skin condition and health. Many other skin parameters—though not detailed here due to space limitations—also exhibited statistically significant improvements.

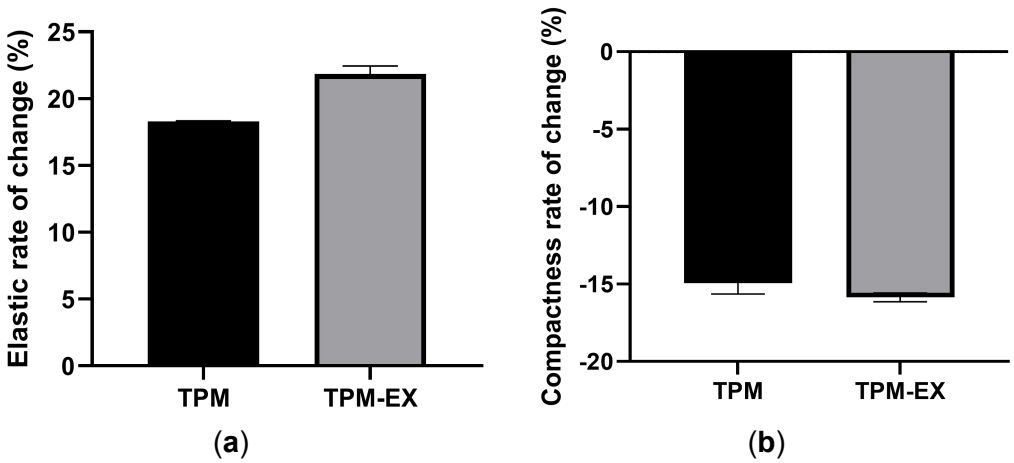

Figure 7. Evaluation of the clinical efficacy of TPM and TPM-EX in vivo. (a) Percentage change in skin elasticity one hour after application in sleep-deprived participants. (b) Percentage change in skin firmness (compactness) one hour after application in sleep-deprived participants.

4. Discussion

As shown in Figure 8, both TPM and TPM-EX effectively improved mitochondrial function at the organelle level, leading to rapid physiological recovery across various cell types and ultimately enhancing skin health in human subjects.

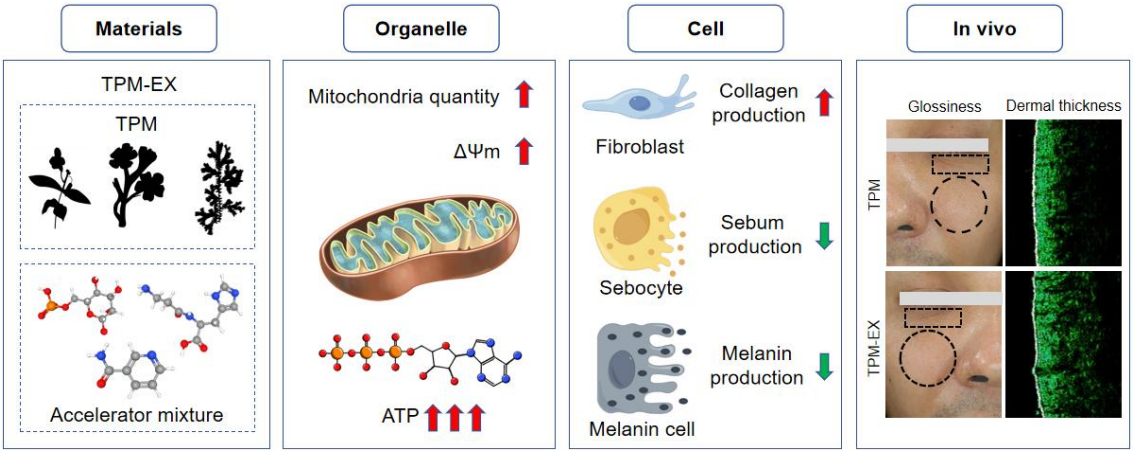

Figure 8. Mechanistic pathway of TPM and TPM-EX from mitochondrial modulation to human clinical effect.

The triple plant-derived mixture, rich in flavonoids, polyphenols, and other bioactive compounds, contributes to enhanced mitochondrial function [20]. TPM increased ATP production by 20.1%, ΔΨm by 262.5%, and mitochondrial quantity by 575.1% ($p < 0.01$). Additionally, it supported cellular homeostasis by boosting type I collagen synthesis by 59.5% in HSFs and reducing sebum secretion by 90.3% in sebocytes.

TPM-EX, when TPM is combined with an accelerator mixture containing carnosine, niacinamide, and sodium mannose phosphate, synergistically enhances mitochondrial bioenergetics through NAD+ biosynthesis and electron transport chain enhancement [21]. In vivo, this formulation showed rapid improvement in sleep-deprived skin, reducing sebum overproduction, dullness, and epidermal thinning within one hour, with sustained efficacy observed over four weeks. This synergy offers a novel approach to anti-aging and metabolic health from within.

5. Conclusion

This dual-component, plant-derived complex not only sustainably enhances mitochondrial function but also revitalizes cellular health by improving cellular bioenergetics and promoting skin regeneration. By combining a potent plant-derived mixture with an accelerator, this eco-conscious formulation addresses a wide range of skin concerns, from boosting collagen synthesis and regulating sebum production to enhancing overall skin elasticity and reducing signs of aging. Leveraging both natural ingredients and cutting-edge biotechnology, this formulation strategy offers a scientifically robust, environmentally friendly solution, setting the stage for next-generation of cosmetics that prioritize both efficacy and sustainability.

6. References

[1] Martic, Ines , et al. "Mitochondrial dynamics and metabolism across skin cells: implications for skin homeostasis and aging." Frontiers in Physiology 14.000(2023):17.
[2] Vasileiou, Panagiotis V. S. , et al. "Mitochondrial Homeostasis and Cellular Senescence." Cells 8.7(2019):686.
[3] Lee, Seo-Eun et al. "Preferred Migration of Mitochondria toward Cells and Tissues with Mitochondrial Damage." International journal of molecular sciences vol. 23,24 15734. 12 Dec. 2022, doi:10.3390/ijms232415734.
[4] Cui, Hang , Y. Kong , and H. Zhang . "Oxidative Stress, Mitochondrial Dysfunction, and Aging." J Signal Transduct 2012.2090-1739(2011):646354.
[5] Maglio, Daniel H. Gonzalez , et al. "Skin damage and mitochondrial dysfunction after acute ultraviolet B irradiation: relationship with nitric oxide production." Photodermatology, Photoimmunology & Photomedicine 21.6(2005).
[6] Yan, et al. "Alcohol induced mitochondrial oxidative stress and alveolar macrophage dysfunction. " BioMed research international (2014).
[7] María J López-Armada, et al. "Mitochondrial dysfunction and the inflammatory response." Mitochondrion 13.2(2013).
[8] Natarajan, V. , et al. "Mitochondrial Dysfunction in Age - Related Metabolic Disorders." Proteomics 20.5a6(2020).
[9] Gao, Xingyu et al. "Telomeres and Mitochondrial Metabolism: Implications for Cellular Senescence and Age-related Diseases." Stem cell reviews and reports vol. 18,7 (2022): 2315-2327. doi:10.1007/s12015-022-10370-8.
[10] Ahmed, Noha S et al. "Impaired Mitochondria Promote Aging-Associated Sebaceous Gland Dysfunction and Pathology." The American journal of pathology vol. 192,11 (2022): 1546-1558. doi:10.1016/j.ajpath.2022.07.006.
[11] Feichtinger, René G et al. "Mitochondrial dysfunction: a neglected component of skin diseases." Experimental dermatology vol. 23,9 (2014): 607-14. doi:10.1111/exd.12484.
[12] Katsuyama, Yushi et al. "Decreased mitochondrial function in UVA-irradiated dermal fibroblasts causes the insufficient formation of type I collagen and fibrillin-1 fibers." Journal of dermatological science vol. 108,1 (2022): 22-29. doi:10.1016/j.jdermsci.2022.10.002.
[13] Zhang, Bei-bei et al. "Mitochondrial membrane potential and reactive oxygen species in cancer stem cells." Familial cancer vol. 14,1 (2015): 19-23. doi:10.1007/s10689-014-9757-9.
[14] Ma, Yi-Shing et al. "Response to the increase of oxidative stress and mutation of mitochondrial DNA in aging." Biochimica et biophysica acta vol. 1790,10 (2009): 1021-9. doi:10.1016/j.bbagen.2009.04.012.
[15] Rodrigues, Tiago, and Letícia Silva Ferraz. "Therapeutic potential of targeting mitochondrial dynamics in cancer." Biochemical pharmacology vol. 182 (2020): 114282. doi:10.1016/j.bcp.2020.114282.
[16] Pochi, P E, and J S Strauss. "Endocrinologic control of the development and activity of the human sebaceous gland." The Journal of investigative dermatology vol. 62,3 (1974): 191-201. doi:10.1111/1523-1747.ep12676783
[17] Chen, WenChieh et al. "Cutaneous androgen metabolism: basic research and clinical perspectives." The Journal of investigative dermatology vol. 119,5 (2002): 992-1007. doi:10.1046/j.1523-1747.2002.00613.x
[18] Brakebusch, Cord, and Reinhard Fässler. "The integrin-actin connection, an eternal love affair." The EMBO journal vol. 22,10 (2003): 2324-33. doi:10.1093/emboj/cdg245.
[19] Choi, Tae-Young et al. "Zebrafish as a new model for phenotype-based screening of melanogenic regulatory compounds." Pigment cell research vol. 20,2 (2007): 120-7. doi:10.1111/j.1600-0749.2007.00365.x.

[20] Rajendran, Kayalvizhi et al. “Emerging trends in nano-bioactive-mediated mitochondria-targeted therapeutic stratagems using polysaccharides, proteins and lipidic carriers.” International journal of biological macromolecules vol. 208 (2022): 627-641. doi:10.1016/j.ijbiomac.2022.03.121.
[21] Katsyuba, Elena et al. ‘‘NAD+ homeostasis in health and disease.’’ Nature metabolism vol. 2,1 (2020): 9-31. doi:10.1038/s42255-019-0161-5.